ACS Biomaterials SCIENCE & ENGINEERING

pubs.acs.org/journal/abseba

Article

Enhanced Neuronal Activity and Asynchronous Calcium Transients Revealed in a 3D Organoid Model of Alzheimer's Disease

Juan Yin and Antonius M. VanDongen*

Cite This: *ACS Biomater. Sci. Eng.* 2021, 7, 254–264

Read Online

ACCESS | Metrics & More | Article Recommendations | Supporting Information

ABSTRACT: Advances in the development of three-dimensional (3D) brain organoids maintained *in vitro* have provided excellent opportunities to study brain development and neurodegenerative disorders, including Alzheimer's disease (AD). However, there remains a need to generate AD organoids bearing patient-specific genomic backgrounds that can functionally recapitulate the key features observed in the AD patient's brain. To address this need, we described a strategy to generate self-organizing 3D cerebral organoids which develop a functional neuronal network connectivity. This was achieved by neuroectoderm induction of human pluripotent stem cell (hPSCs) aggregates and subsequent differentiation into desired neuroepithelia and mature neurons in a 3D Matrigel matrix. Using this approach, we successfully generated AD cerebral organoids from human pluripotent stem cells (hPSCs) derived from a familial AD patient with a common mutation in presenilin 2 (PSEN2^{N141I}). An isogenic control with an identical genetic background but wild-type PSEN2 was generated using CRISPR/Cas9 technology. Both control and AD organoids were characterized by analyzing their morphology, the Aβ42/Aβ40 ratio, functional neuronal network activity, drug sensitivity, and the extent of neural apoptosis. The spontaneous activity of the network and its synchronization was measured in the organoids via calcium imaging. We found that compared with the mutation-corrected control organoids, AD organoids had a higher Aβ42/Aβ40 ratio, asynchronous calcium transients, and enhanced neuronal hyperactivity, successfully recapitulating an AD-like pathology at the molecular, cellular, and network level in a human genetic context. Moreover, two drugs which increase neuronal activity, 4-aminopyridine (4-AP) and bicuculline methochloride, induced high-frequency synchronized network bursting to a similar extent in both organoids. Therefore, our study presents a promising organoid-based biosystem for the study of the pathophysiology of AD and a platform for AD drug development.

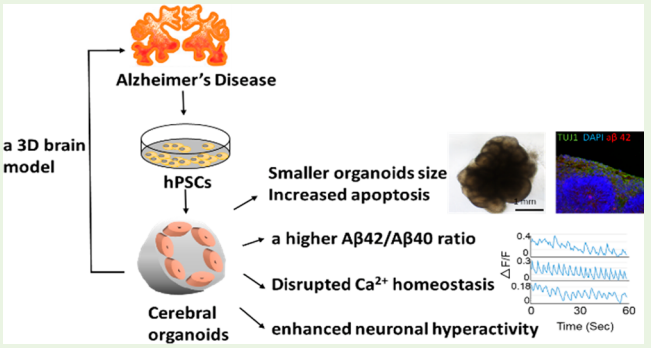

KEYWORDS: *Alzheimer's disease, 3D organoid model, neuronal activity, presenilin 2*

INTRODUCTION

Alzheimer's disease (AD) is the most prevalent cause of dementia, characterized by a progressive loss of both synaptic function and long-term memory formation.[1] Although many efforts have been made to develop therapeutic drugs in the past decades, there is currently no treatment that could prevent, stabilize, or reverse the progression of this disease.[2] Therefore, a detailed understanding of the pathophysiology underlying AD and the development of novel therapeutics are highly desirable. However, this remains quite challenging due to the experimental inaccessibility of the functional human brain.[3] Instead, *in vitro* model systems offer alternative unprecedented opportunities to study AD, as they can recapitulate faithfully some key features involved in AD pathophysiology.[4]

Animal model studies, performed mainly on rodents, have greatly improved our understanding of the mechanisms underlying AD, but animal models have flaws as well. For example, mice cannot spontaneously develop neurofibrillary tangles, accelerated phenotypes and sporadic pathology that are observed in human AD brains during aging,[5−7] which suggests that the molecular networks driving AD initiation may be different between humans and mice. These discrepancies indicate a great demand for paradigms that allow investigations into AD in a "human context".[8] Advanced human pluripotent stem cell (hPSC) technology provides such an opportunity to address this challenge. It has been shown that neurons differentiated from patient-derived hPSCs could exhibit typical features of AD pathology, such as amyloid plaques and neurofibrillary tangles,[9,10] which enables the exploration of this disease using human cells. However, two-dimensional (2D) cultures of hPSCs are subjected to some inherent limitations.

Received: November 7, 2020
Accepted: December 14, 2020
Published: December 21, 2020

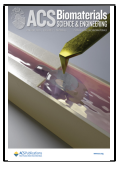

https://dx.doi.org/10.1021/acsbiomaterials.0c01583
ACS Biomater. Sci. Eng. 2021, 7, 254–264

For example, this method fails to reproduce sophisticated cell−cell interactions in the brain.[11] The phenotypes of aberrant extracellular protein aggregation in AD could not be reproduced perfectly due to the lack of an interstitial compartment in the 2D culture.[12] Therefore, several groups have developed methodologies to generate cultures of three-dimensional (3D) cerebral organoids.[13−15] Compared with 2D cultures, organoids are considered to be excellent models to study brain development, disease progression, and perform drug evaluation due to their ability to differentiate, self-organize, and form structures that are highly reminiscent of the cerebral cortex.[16−18] Significantly, AD organoids generated from familial AD patients with genetic mutations in presenilin 1 (PSEN1) or the amyloid precursor protein (APP) have shown the great potential in AD modeling due to their convenience, reproducibility, and scalability. Many key phenotypes of AD, such as amyloid aggregation, hyperphosphorylated tau protein, endosome abnormalities, and neurofibrillary tangles, could be recapitulated in these organoids.[5,16,17,19] As a homologue to PSEN1, the presenilin 2 (PSEN2) gene encodes the catalytic components of the γ-secretase enzyme that promotes the final cleavage of APP to generate Aβ.[20,21] The PSEN2 mutation is also causally related with the pathogenesis of AD by greatly increasing intracellular aggregation-prone Aβ42 production.[22] But so far, the study on organoids carrying a patient-specific genome with PSEN2 mutation and the isogenic control have not been reported yet. Moreover, in previously studied miniature 3D models, recapitulation of the abnormal functional aspects of AD pathology has been less well studied. To this end, we aim to develop such an unexplored AD organoids-based model that can harbor typical functional network activity of a patient's brain, which will substantiate the great potential of this model as a useful tool to study AD or drug evaluation. Herein, we used hPSCs derived from a familial AD patient bearing a PSEN2 gene mutation to generate AD organoids and the isogenic control organoids, respectively, and analyzed the morphology, protein marker expression, functional neuronal activity of both organoids, and their drug sensitivity, successfully developing improved AD organoids that can functionally mimic human brain in terms of neuronal network activity.

METHODS

Maintenance and Characterization of hPSCs. hPSCs were obtained from the Coriell Institute for Medical Research under their consent and privacy guidelines as described on their website (http://catalog.coriell.org/). The hPSCs carrying PSEN2^{N141I} point mutation is CS08iFAD-nxx (https://web.expasy.org/cellosaurus/CVCL_YX93) and control hPSCs is CS00iCTR. AD hPSCs were derived from an 81-year-old female AD patients's fibroblasts using an episomal plasmid vector. The AD patient had a heterozygous mutation of PSEN2 (p.Asn141Ile (c.422A>T)). Control hPSCs were derived from a healthy 61-year-old male's fibroblasts using an episomal plasmid vector. Both AD hPSCs and control hPSCs had a normal karyotype (46, XX Normal Female or 46, XY Normal Male). hPSCs colonies were grown on Matrigel (Catalog #354277, Corning) in TeSR medium (mTeSR1, Catalog #85850, STEMCELL Technologies) according to the manual. Pluripotency was assessed by immunostaining with surface and nuclear pluripotency markers (SSEA-1 and Nanog, Catalog #ab109884, Abcam) for subsequent imaging.

CRISPR/Cas9-Mediated Correction of the PSEN2^{N141I} Mutation. The gene-corrected isogenic control lines (i-Control) were generated from AD hPSC lines using a previously published donor plasmid-mediated CRISPR/Cas9 protocol.[23] The sgRNA vector (Cas9 sgRNA vector, Plasmid #68463), donor plasmid (PL552, Plasmid #68407), and Cas9 nickase plasmid (pCas9D10A_GFP, Plasmid #44720) were purchased from Addgene. We designed two pairs of sgRNA, which targeted the intron beside the exon 3 (Table S1). The donor plasmid, two pairs of sgRNA vectors, and Cas9 nickase plasmid were transduced into the AD hPSCs by using Human Stem Cell Nucleofector Kit 1 (Lonza VPH-5012). Three days after electroporation, puromycin (0.5 μg/mL, Invivogen) was added into hPSC medium for selection for 2 weeks. Then, individual colonies were picked up and identified by genomic PCR.

Genomic DNA Extraction and Genomic PCR. Genomic DNA was extracted with QuickExtract DNA Extraction Solution (Epicenter, QE09050). Genomic PCR was carried out using Q5 High-Fidelity DNA Polymerase (New England Biolabs, M0492L).

Generation of Organoids. The cerebral organoids were generated from hPSCs using STEMdiff Cerebral Organoid Kit (Catalog #08570, STEMCELL Technologies) according to the protocol provided by STEMCELL Technologies, and only a small part of the method was modified. In brief, organoids were generated from hPSCs in four stages: embryonic body (EB) formation, neuroectoderm induction, neuroepithelia expansion, and organoid maturation. At stage 1, hPSCs were dissociated into single cells in Dispase (1 U/mL, Catalog #07923, STEMCELL Technologies) and quickly reaggregated using low-cell-adhesion-coated 96-well plates with V-bottomed conical wells (Corning) in EB Formation Medium (12 000 cells per well, 100 mL) containing 10 μM Y-27632. Fresh EB Formation Medium without Y-27632 was changed every other day. At stage 2, EBs were fed with induction medium to induce differentiation of the primitive neuroepithelia. At 6 days, EBs were moved to 24-well ultralow attachment plates (Corning) in Induction Medium. At stage 3, the neuroepithelial tissues were embedded into droplets supported by a 3D matrix composed of Matrigel in which organoids expanded to develop neuroepithelia and showed proliferation of neural progenitors. At 8 days, EBs were embedded with Matrigel (Catalog #354277, Corning) and changed to 6-well ultralow attachment plates (Corning) in Expansion Medium. At stage 4, Matrigel drops were cultured in the maturation medium to elongate the neuroepithelial tissues. At 11 days, the medium was replaced with Maturation Medium, and plates of organoids were placed on an orbital shaker in an incubator (37 °C, 5% CO_2). The organoids were imaged using a motorized inverted wide-field epifluorescence microscope (Nikon Eclipse Ti-E) at different stages of development. At least three independent experiments were performed for each condition. The diameters of organoids were measured using NIS Elements AR version 4.1 software (Nikon).

Dissociation of Organoids into Single Cells. Whole cerebral organoids were washed three times in 1× PBS and dissociated in 2 mL of Accutase (Gibco) containing 0.2 U/μL Dnase I (Roche) for 45 min at 37 °C. Cells were collected by centrifugation at 300*g* for 5 min and resuspended in 10 mL of neural culture media (Neurobasal medium, 1× B-27, 200 mM L-glutamine, 50 U/mL penicillin, and 50 mg/mL streptomycin). Then, centrifugation was performed at 300*g* for 5 min, and cells were resuspended in neural culture media. Cell viability was assessed by Trypan blue staining (typically 85−95% viable) and counted using an automatic cell counter (Bio-Rad). Cells were plated on 100 mg/mL poly-L-ornithine and 10 mg/mL laminin coated plates at 50 000 cells/cm^2 and incubated overnight. The medium was changed twice a week.

Cryosectioning and Immunostaining for Organoids. Organoids were fixed with 4% paraformaldehyde (PFA) overnight at 4 °C and then transferred to 30% sucrose solution. After organoids sank in the sucrose solution overnight at 4 °C, they were embedded in O.C.T. (Sakura, Tokyo, Japan) and sliced in a cryostat (20 μm slices). Following air drying for 30 min, the slides containing the sliced samples were permeabilized with 0.1% triton X-100 for 20 min and blocked with 10% donkey serum in PBS for 1 h at room temperature. The slides were incubated with antibody (Table S2) for 1 h at room temperature. Next, the slices were washed with PBST (PBS with 0.05% triton X-100) and incubated with antimouse or rabbit antibody (Table S3) for 30 min at room temperature. The nuclei were stained

https://dx.doi.org/10.1021/acsbiomaterials.0c01583
ACS Biomater. Sci. Eng. 2021, 7, 254−264

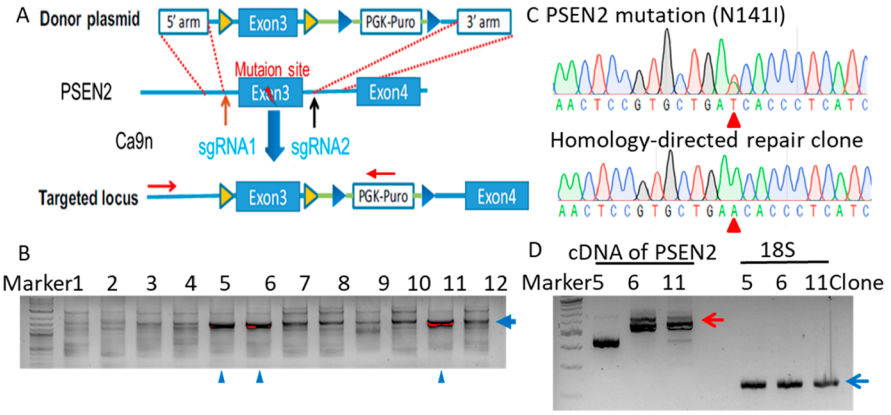

Figure 1. CRISPR/Cas9-mediated correction of PSEN2^{N141I} hPSCs lines. (A) Schematic depiction of the targeting strategy for exon 3 of the PSEN2 locus. Vertical arrows indicate sgRNA1 and sgRNA2 targeting sites. The genotyping PCR primers are indicated (red arrows). Donor plasmids: PGK, phosphoglycerate kinase promoter; Puro, puromycin-resistance gene. (B) PCR genotyping of hPSC clones targeted by both sgRNA1 and sgRNA2. PCR products for the correctly targeted PSEN2 locus are 1300 bp (blue arrows). One targets the intron, and the other targets the PGK-Puro. Clone 5, 6, and 11 are selected to sequence. (C) Representative sequencing results of PSEN2 mutation (upper) and homology-directed repair clone (lower). A heterozygous substitution (A>T at nucleotide 787) in PSEN2 gene results in an Asn141Ile (N141I) missense mutation. (D) RT-PCR analysis of cDNA of PSEN2. The red arrow indicates the full length of cDNA. The blue arrow indicates cDNA of 18S.

using the DAPI solution (1 μg/mL). The slides were mounted and analyzed using a fluorescence microscope.

Immunohistochemistry. For immunostaining of hPSCs and neurons, cells were fixed with 4% PFA directly on the 35 mm cell culture dish for 1 h and then washed three times with PBS. The cells were treated with PBS containing 1% Triton X-100 for 15 min. Then, cells were incubated in the blocking solution (PBS with 0.1%Triton X-100 plus 10% donkey serum) for 30 min at room temperature. The antibody (Table S4) was diluted in the blocking solution, which was then added to the culture dish for incubation for 1 h at room temperature. Cells were washed four times with PBST and treated with antimouse or rabbit antibody (Table S5) for 1 h at room temperature. Then, cells were washed four times with PBST and incubated with DAPI (1 μg/mL, diluted in PBS) for 10 min at room temperature for nuclear counterstain. Cells were visualized using a confocal microscope under 20× magnification.

Calcium Imaging of the Neuronal Network. For calcium dye loading, the cells were incubated with 10 mM Fluo-4-AM solution (Catalog #F14201, Invitrogen) and 0.04% Pluronic F-127 (Catalog #P3000MP, Invitrogen) for 1 h in an incubator (37 °C, 5% CO_2). Excess dye was removed by washing with culture medium three times. Imaging was carried out at 37 °C and 5% CO_2 using a confocal microscope (Nikon). Time-lapse image sequences were acquired at no intervals for 2 min. The fluorescence change over time is defined as $\Delta F/F = (F - F_{basal})/F_{basal}$, where F is the fluorescence at any time point and F_{basal} is the minimum fluorescence of each cell. A neuron was considered active if calcium transients were observed at least once during the total imaging period. For pharmacological experiments, after 2 min of time-lapse image, organoids were treated with bicuculline methochloride (50 μM) and 4-aminopyridine (4-AP) (10 μM). Imaging data were taken another 5 min after bicuculline methochloride or 4-AP treatment in the same field. Tetrodotoxin (500 nM) was added into the culture medium, and Ca^{2+} images were taken.

Statistical Analysis. All statistical analyses were performed using the unpaired t test. Data in graphs are expressed as mean values ± SEM. Error bars represent SEM.

RESULTS

Patient and Control Cells. The linkage of a locus on human chromosome 1q31−42 to early onset familial AD led to the identification of the point mutation PSEN2^{N141I} (422A>T) in the Volga German kindreds in 1995.[24] The AD hPSC lines were collected from a female familial AD patient carrying a heterozygous PSEN2^{N141I} point mutation. The control hPSC lines were collected from a healthy person who was about the same age as the AD patient. The AD hPSC and control hPSC lines were purchased from Cedars Sinai (ID: CS08iFAD-nxx and CS00iCTR). Both hPSC lines were identified and confirmed by the detection of expression of pluripotency-associated markers, including Nanog and SSEA-1 by immunostaining (Figure S1).

CRISPR/Cas9-Mediated Correction of PSEN2^{N141I} Mutation in Isogenic Control Cells. To examine the cause−effect relationship between the PSEN2^{N141I} point mutation and AD phenotypes, we generated gene-corrected isogenic control lines (termed as i-Control) from AD hPSC lines using a previously published donor plasmid-mediated CRISPR/Cas9 workflow.[23] In brief, we designed two pairs of sgRNAs that target unique sequences in the introns flanking exon 3 of the PSEN2 gene (Figure 1A). The donor plasmid contains the 5′ and 3′ arm, which are the homologous regions of the introns flanking exon 3 of the PSEN2 gene, and one PGK-puromycin cassette. We then transfected hPSCs with donor plasmid and the Cas9 nickase (Cas9n) plasmid, along with both sgRNA1 and sgRNA2. After drug selection, PCR genotyping and sequencing showed that about 25% of the clones were targeted to at least one allele (Figure 1B and C). The integrity of the cDNA was verified by RT-PCR and DNA sequencing (Figure 1D). Finally, the successfully corrected clones, whose genomic background was the same as that of the AD hPSC line, were expanded and used to generate organoids (termed as i-Control organoids).

Generation of Cerebral Organoids. Several protocols have been developed to generate cerebral organoids from hPSCs;[25−29] we followed the protocol which is provided by Stemcell Technologies. We generated organoids from three hPSC lines, which included two control hPSC lines (the above control line from a healthy individual and the i-Control with the corrected gene mutation, respectively) and one hPSC line bearing the PSEN2^{N141I} mutation. These organoids gradually underwent embryonic body (EB) formation, neuroectoderm induction, neuroepithelia expansion, and organoid maturation

https://dx.doi.org/10.1021/acsbiomaterials.0c01583
ACS Biomater. Sci. Eng. 2021, 7, 254−264

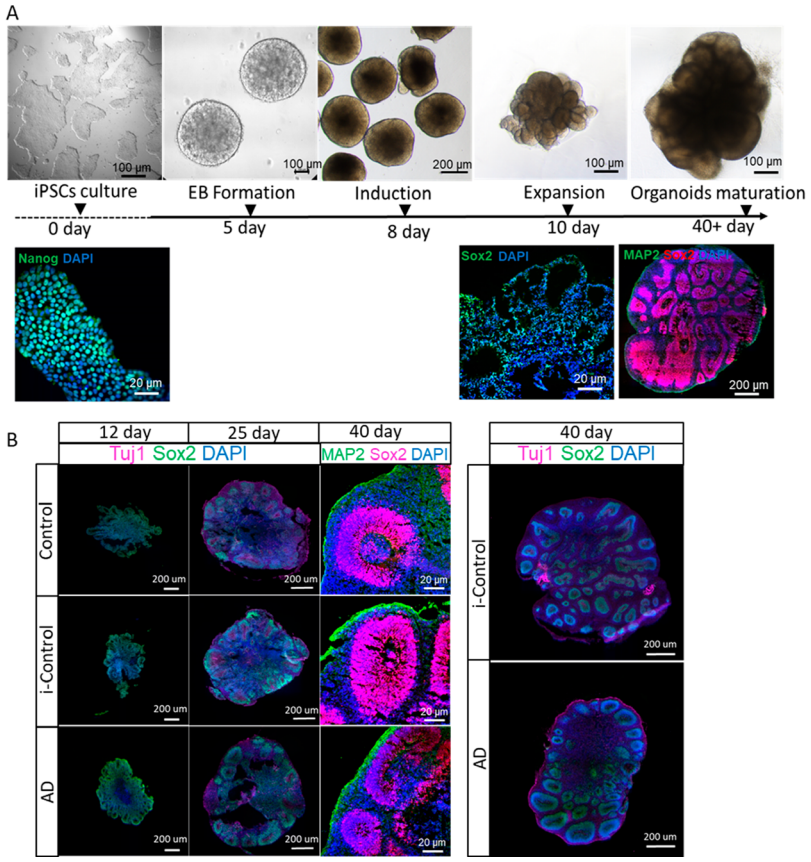

Figure 2. Organoids recapitulate organization of the cerebral cortex. (A) Schematic of the culture system used to generate human cerebral organoids from hPSCs. Representative immunostaining images (lower panel) showed the pluripotent state of hPSCs (Nanog), neural progenitor cells (Sox2), and neurons (MAP2) in organoids, respectively. (B) Sectioning and immunohistochemistry showing complex neuroepithelial tissues containing neural progenitors (Sox2), neurons (TUJ1), and nuclei (DAPI) at days 12, 25, and 40 in the control, i-Control, and AD organoids.

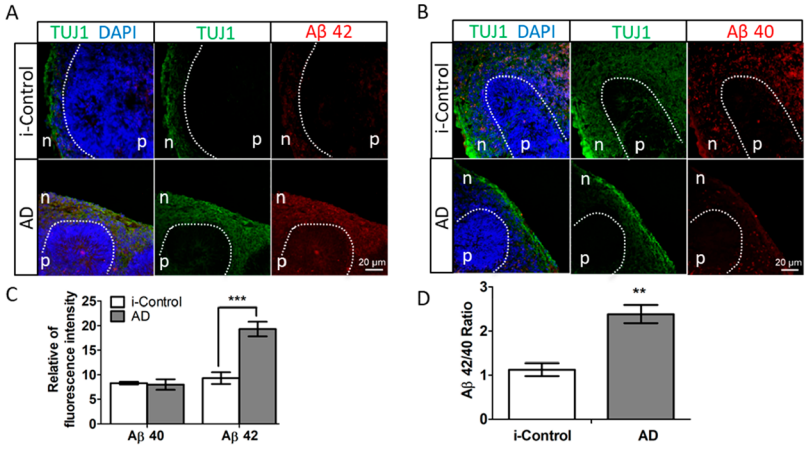

Figure 3. Ratio of Aβ42/Aβ40 was elevated in AD organoids. (A) Sectioning and immunohistochemistry showing the expression of Aβ42 at neuroepithelial tissues on day 45. The nucleus was stained with DAPI, and neurons were stained with TUJ1 (n: neurons; p: neural progenitors; the neural progenitors are circled by the dotted line). (B) Sectioning and immunohistochemistry showing the expression of Aβ40 at neuroepithelial tissues on day 45. The nucleus was stained with DAPI, and neurons were stained with TUJ1 (n: neurons; p: neural progenitors; the neural progenitors are circled by the dotted line). (C) Quantification of expression level of Aβ40 and Aβ42. The fluorescence intensity of Aβ40 and Aβ42 was analyzed by ImageJ (n = 7, ***P < 0.001). (D) Quantification of Aβ 42/40 ratio (n = 7, **P < 0.01).

(Figure 2). Neurons and progenitors were successfully identified in a large continuous cortical tissue within an organoid after 40 days of incubation in the maturation medium (Figure 2A). Immunostaining showed that the organoids generated from AD hPSCs bearing the PSEN2^{N141I} mutation can develop several continual cortical tissues, and their structures were not significantly different from those of organoids generated from control and i-Control hPSCs. At day 12, almost all the cells in the organoids were neural progenitor cells marked by Sox2 expression. At day 25, occasional neurons were visible in the organoids, marked by Tuj1 expression. The organoids progressively produced more

https://dx.doi.org/10.1021/acsbiomaterials.0c01583
ACS Biomater. Sci. Eng. 2021, 7, 254−264

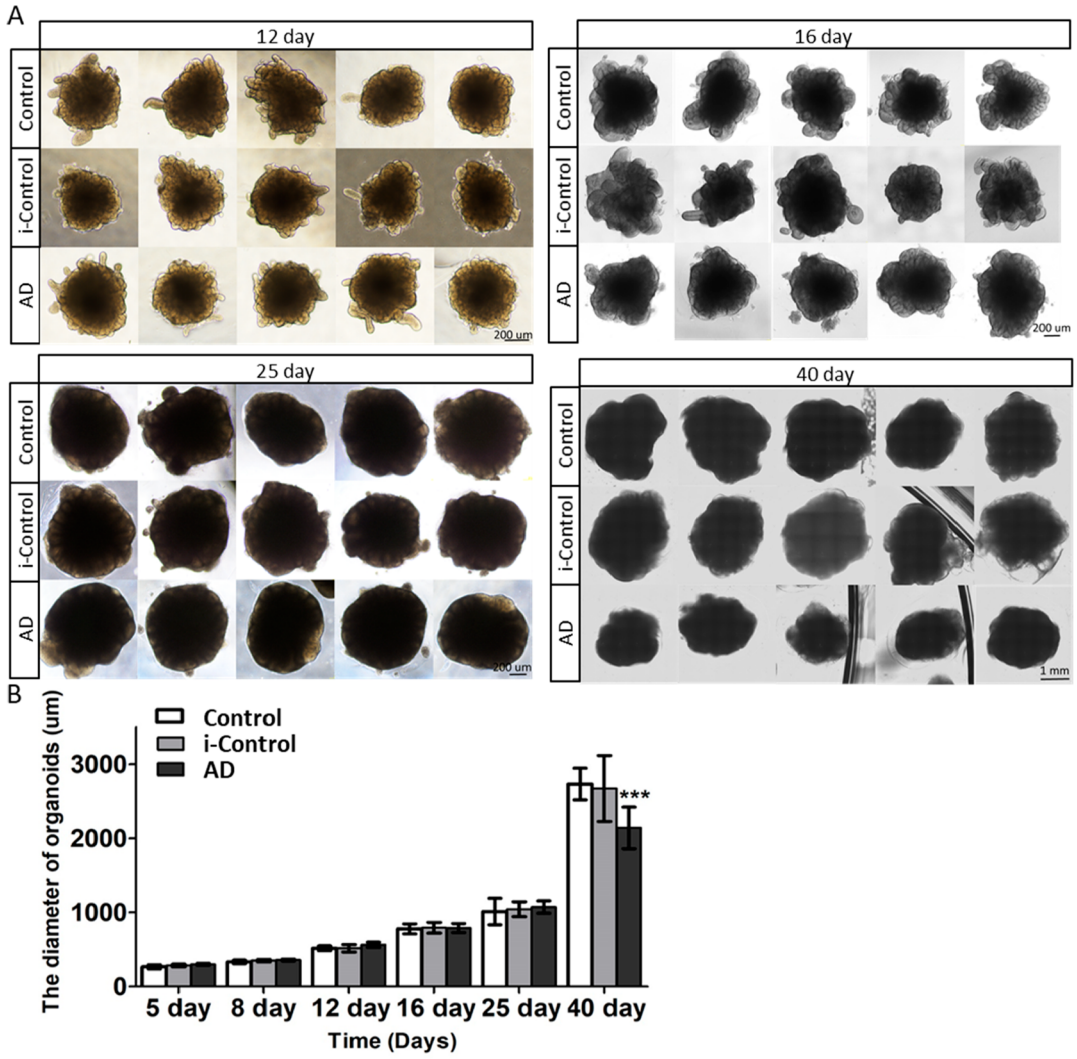

Figure 4. Size of organoids at different development stages. (A) Phase-contrast images of organoids at day 12, 16, 25, and 40. (B) Quantification of the size of organoids by measuring the diameters of organoids (n = 15, ***p < 0.001).

neurons and thickened cerebral tissues over the subsequent 1 month (Figure 2B).

AD Phenotypes in 3D Organoids. Previous studies of the effect of the PSEN2^{N411I} mutation in human brain, cerebrospinal fluid, and plasma, as well as in transgenic animals and cellular systems showed that the ratio of Aβ42/Aβ40 was consistently elevated.[30] An increased production of Aβ42 is a major hallmark in the brains of patients with AD, as the higher concentration of Aβ42 oligomers is toxic to neurons.[22] Therefore, to determine whether the organoids generated in our work can recapitulate this key pathogenic feature of AD, we tested the expression level of Aβ40 and Aβ42 and found that Aβ42 was significantly increased, while Aβ40 was almost unchanged compared to i-Control organoids (Figure 3A−C and Figures S2 and S3). Quantification showed that the ratio of Aβ42/Aβ40 was significantly increased (Figure 3D). These data demonstrated that AD organoids bearing the PSEN2^{N141I} mutation could recapitulate an AD-like feature: toxic protein accumulation.

AD Organoids Were Smaller than i-Control Organoids Due to an Increase in Apoptosis. At early differentiation stages, the morphology of organoids generated from control, i-Control, and AD hPSCs did not show significant differences. All organoids developed enlarged neuroepithelia, as evidenced by budding at the EB surface. After 40 days, they all exhibited dense cores with regions of organoids displaying optically translucent edges. However, the AD organoids were smaller than organoids generated from control and i-Control hPSCs (Figure 4A and B). Next, to more precisely analyze the effect of the PSEN2 mutation on the defective morphology of AD organoids, i-Control and AD organoids were compared and characterized in the following studies because they are isogenic. This may minimize the unknown effects caused by different genetic backgrounds of control organoids derived from different healthy individuals.

In previous studies, it was found that AD mouse models showed a significant reduction of cell proliferation in neurogenic niches at early stages of development.[31] Therefore, we decided to test whether the smaller size of AD organoids was caused by a reduced cell proliferation. Immunostaining for the expression of cell proliferation markers showed that more cells were positive for the proliferation marker Ki67 at early stage (day 16) than that at later stage (day 45) in both i-Control and AD organoids (Figure 5A). This suggested that there were more neural progenitors in the early stages of organoid development as mature neurons lost their ability to

https://dx.doi.org/10.1021/acsbiomaterials.0c01583
ACS Biomater. Sci. Eng. 2021, 7, 254−264

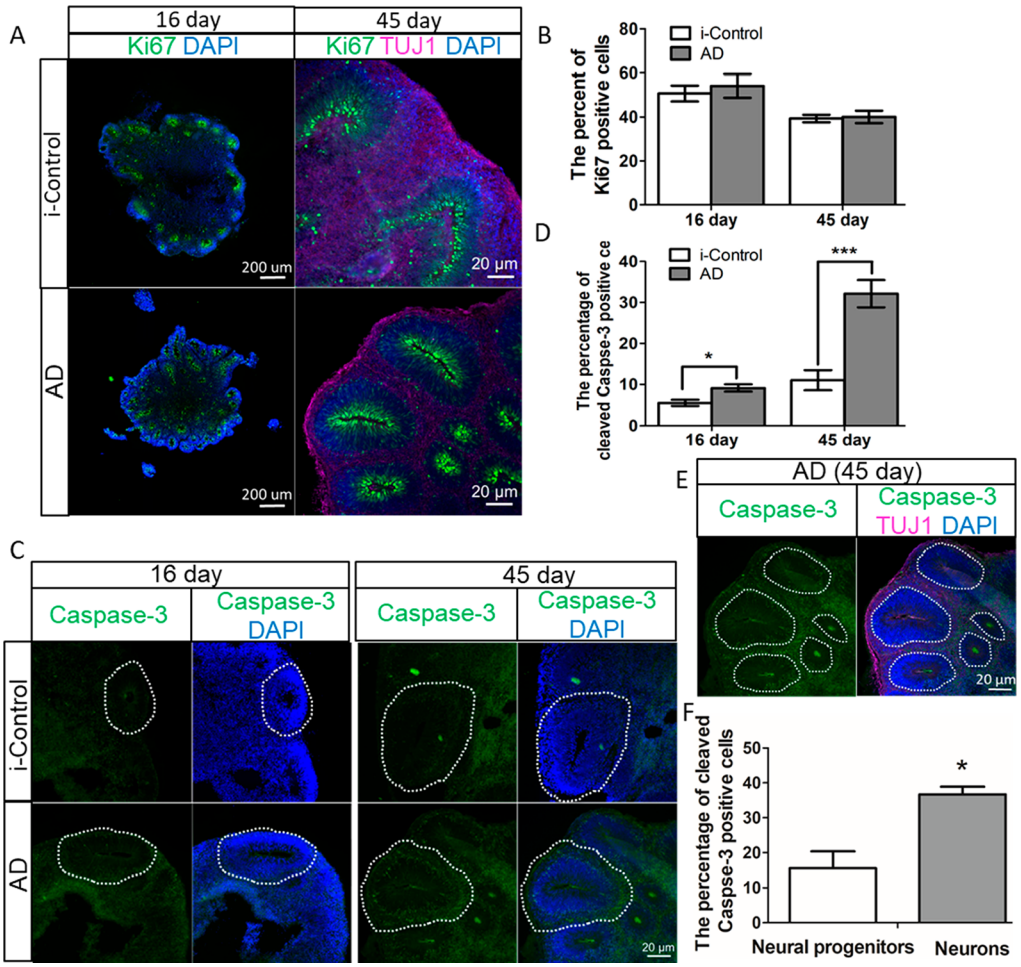

Figure 5. Image analysis of cerebral organoids. (A) Sectioning and immunohistochemistry showing the expression of Ki67 at neuroepithelial tissues at day 16 and 45 in i-Control and AD organoids. (B) Quantification of expression level of Ki67 (n = 3) in the i-Control and AD organoids. (C) Sectioning and immunohistochemistry showing the expression of cleaved caspase-3 at neuroepithelial tissues (dotted line) at day 16 and 45 in i-Control and AD organoids. (D) Quantification of expression level of cleaved caspase-3 (n = 3, $^*P < 0.05$, $^{***}P < 0.001$) in the i-Control and AD organoids. (E) Sectioning and immunohistochemistry showing the expression of cleaved caspase-3 at neuroepithelial tissues (dotted line) at day 45 in the AD organoids. Neurons (TUJ1, red) and nucleus (DAPI, blue). (F) Quantification of expression level of cleaved caspase-3 in the mature neurons and neural progenitor cells in AD organoids at day 45 (n = 3, $^*P < 0.05$).

proliferate, which is consistent with the result shown in Figure 2B. But statistical analysis showed that there was no difference in cell proliferation rate between i-Control and AD organoids at the same growth stage (day 16 or 45) (Figure 5B).

In the clinic, AD is characterized by marked neuronal loss and brain atrophy.[32−34] Previous studies of expression of apoptosis markers demonstrated that both wild-type and mutant PSEN2 could trigger apoptosis in a wide range of cell lines, including human HEK293 cells and murine neurons.[35] To determine whether this phenotype was maintained in AD organoids, we measured the expression of a cell apoptosis marker (cleaved caspase-3) at different growth stages. At day 16, there are only a few cells stained positive for cleaved caspase-3 in both i-Control and AD organoids, but the activity of cleaved caspase-3 in the AD organoids was slightly higher than that in the i-Control. At day 45, compared with the i-Control, neurons exhibited dense cleaved caspase-3 staining over a larger area in the AD organoids, showing that the activity of cleaved caspase-3 in AD organoids was significantly higher than those derived from i-Control hPSCs (Figure 5C and D). Moreover, the intensity of detected green fluorescence signals inside the region of organoids was much stronger than that in the peripheral region (Figure 5C), indicating that more healthy neurons were located along the perimeter of organoids while centrally located cells had much higher apoptosis activity, which may be caused by the poor availability of nutrients, oxygen, and growth or neurotropic factor gradients inside the organoids.[36] Therefore, these results show that much higher apoptosis may account for the defect in the morphology of AD organoids, resulting in a smaller size.

Calcium Homeostasis Was Disrupted in AD Organoids. After characterizing their morphology and protein marker expression, we continued to characterize the functional neuronal network activity in the i-Control and AD organoids. Accumulating evidence has shown that PSEN2 mutations can disrupt calcium signaling, resulting in neurodegeneration in AD.[37,38] Therefore, we measured Ca^{2+} oscillations to analyze the calcium homeostasis in both organoids by using a fluorescent calcium indicator (Fluo-4). To better observe the cells inside the organoids, we cut the organoid into two halves and plated one-half on a culture dish at day 40 (Figure 6A). The neurons migrated and spread out to form a single cell layer around the periphery of the organoids (Figure 6B). Spontaneous calcium dynamics were detected in the migrated

https://dx.doi.org/10.1021/acsbiomaterials.0c01583
ACS Biomater. Sci. Eng. 2021, 7, 254−264

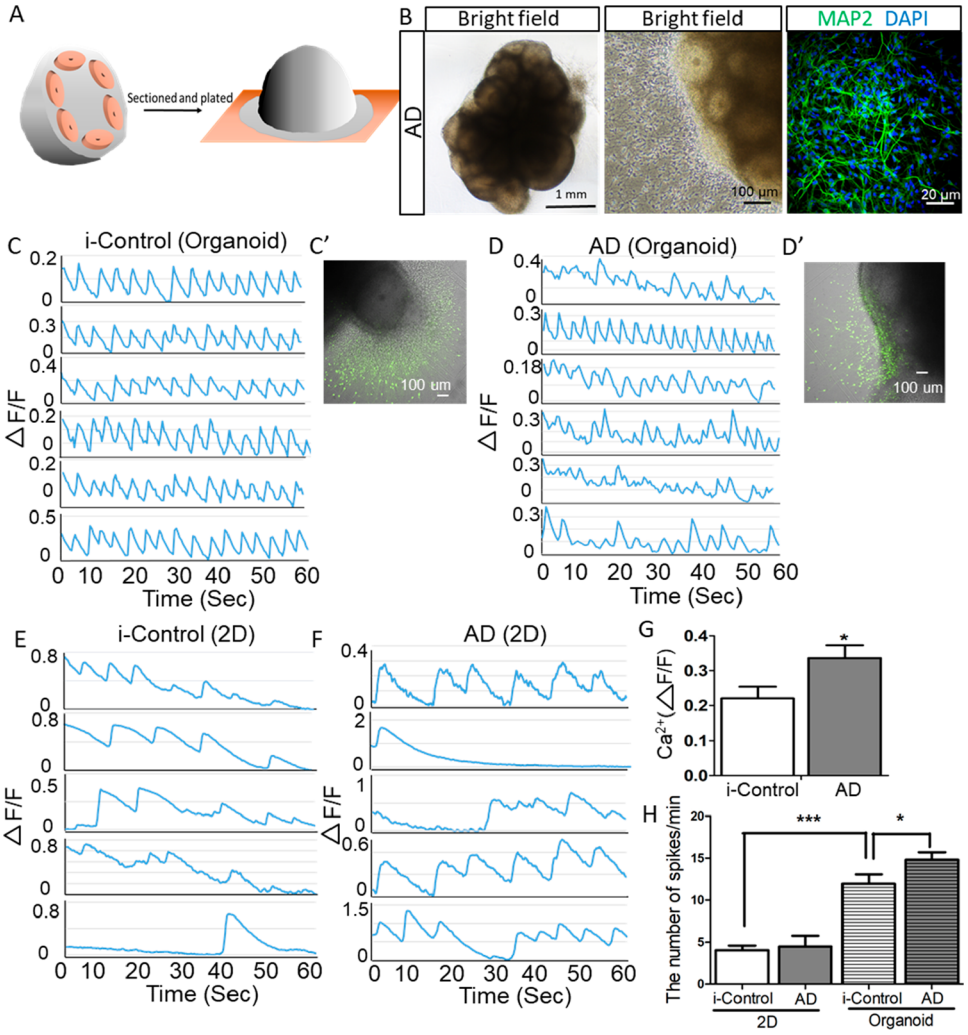

Figure 6. Analysis of calcium activity in cerebral organoids. (A) Schematic depiction of cutting the organoid and plating one-half of it on the plate at day 40. (B) Left panel: Bright field images of whole organoids. Middle panel: Bright field image of half of an organoid that was cultured on a 35 mm glass bottom dish for 3 weeks showing neurons that have migrated out from the surface of the organoid. Right panel: immunohistochemistry staining of neurons migrating away from the organoids. Nuclei were stained with DAPI, and neurons were stained with TUJ1. (C) Single-cell tracings of spontaneous calcium surges in the migrated neurons from i-Control organoids (regions of interest shown in C′) as measured by change in fluorescence (arbitrary units). (D) Single-cell tracings of spontaneous calcium surges in the migrated neurons from AD organoids (regions of interest showed in D′) as measured by change in fluorescence (arbitrary units). (E) Single-cell tracings of spontaneous calcium surges in dissociated neurons from isogenic control organoids. (F) Single-cell tracings of spontaneous calcium surges in dissociated neurons from AD organoids. (G) Quantification of average normalized calcium responses for baseline in isogenic control organoids and AD organoids (n = 5, $^*P < 0.05$). (H) Quantification of the numbers of spikes per minute (n = 15, $^*P < 0.05$, $^{***}P < 0.001$).

neurons after three weeks in culture. Imaging data are presented by calculating relative changes in fluorescence ($\Delta F/F$) in regions of interest corresponding to neurons. Interestingly, whereas i-Control organoids displayed synchronized calcium transients typically reported for cultured neuronal networks, the calcium transients from AD organoids lacked synchronization (Figure 6C and D and Figure S4). However, AD organoids were more active than i-Control organoids (Figure 6H). These data suggest that the PSEN2^{N141I} mutation may enhance neuronal hyperactivity. At the same time, we found that the amplitudes of spontaneous Ca^{2+} transients in PSEN2^{N141I} mutation organoids were significantly higher than those in the i-Control organoids (Figure 6G). To further confirm that this functional behavior was caused by the organized 3D cell assembly, the floating organoids were redissociated into single cells to generate a monolayer culture with the purpose to test the Ca^{2+} transients at the 2D cell level (Figure S5). However, after three weeks of culture, the calcium homeostasis patterns displayed in the organoids were lost in 2D. There were no significant differences in the activity patterns, such as the synchronicity and numbers of spikes, between i-Control and AD neurons (Figure 6E and F). Moreover, the frequency of Ca^{2+} spikes was also significantly lower in the 2D cultures than in the 3D organoids (Figure 6H). Taken together, these data indicate that neuronal networks are better organized in organoids than in monolayer cultures, as more spontaneous Ca^{2+} transients could be detected in organoids. This experimental evidence indicates that organoids have advantageous potential to be used as a functional and "information-rich" *in vitro* model to study AD.

Effect of Drug Treatment on Spontaneous Ca^{2+} Transients in Organoids. To further analyze the effect of the PSEN2^{N141I} point mutation on dynamic changes of the spontaneous Ca^{2+} transients, two types of drugs were used

https://dx.doi.org/10.1021/acsbiomaterials.0c01583
ACS Biomater. Sci. Eng. 2021, 7, 254−264

(Figure 7A). 4-AP is an A-type potassium channel blocker that can induce epileptiform activity in the rat hippocampus.[39] In

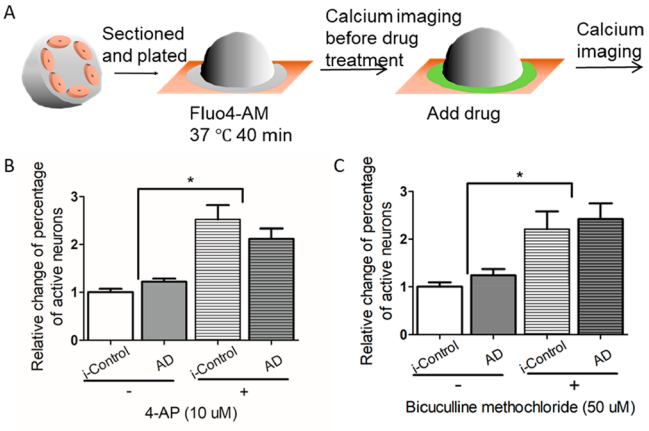

Figure 7. Analysis of calcium activity in organoids after drug treatment. (A) Schematic depiction of the drug load test. (B) The relative change of percentage of active neurons after 4-AP treatment (n = 15, *P < 0.05). (C) The relative change of percentage of active neurons after bicuculline methochloride treatment (n = 15, *P < 0.05).

our assay, we observed that the frequency of spikes was increased about 2-fold by addition of 10 μM 4-AP in both i-Control and AD organoids, but there was no significant difference between them before or after drug treatment (Figure 7B). Bicuculline methochloride is a GABA receptor antagonist which increases the activity of neuronal networks in organoids.[40] Similar to the organoids treated by 4-AP, the frequency of spikes was also increased about 2-fold after adding 50 μM bicuculline methochloride, but there was also no obvious difference in i-Control and AD organoids before or after drug treatment (Figure 7C). Finally, we also treated the organoids with tetrodotoxin (TTX), which is a sodium channel blocker that can inhibit the firing of action potentials in neurons.[41] We observed the silencing of Ca^{2+} spikes, indicating that spontaneous Ca^{2+} transients were dependent upon neuronal activity (Figure S6). These results suggest that although both 4-AP and bicuculline methochloride can induce spontaneous Ca^{2+} transients in both organoids, PSEN2 mutations may have no significant effect on their drug sensitivity.

DISCUSSION

In this contribution, we generated functional cerebral organoids from AD patient-derived hPSCs bearing the $PSEN2^{N141I}$ point mutation and the gene-corrected isogenic control cell lines, which was obtained by using the CRISPR/Cas9 system. Our data clearly show that organoids with the $PSEN2^{N141I}$ point mutation could successfully recapitulate several key features of AD pathology, including an increased Aβ42/Aβ40 ratio and dysfunctional neuronal network activity.

Previous studies on organoid modeling of brain development and neurodegenerative disorders revealed that certain types of disease-derived organoids exhibited a smaller overall organoid size compared to control organoids.[42] For example, organoids derived from Miller−Dieker syndrome, autosomal recessive primary microcephaly, and Aicardi−Goutieres syndrome were smaller than the control organoids, which was caused by a decrease in neural progenitor proliferation or an increase in neuronal apoptosis.[41,43,44] Unexpectedly, in our study, we found that a morphological defect occurred in AD organoids bearing PSEN2 mutation after 40 days in culture. Compared to i-Control organoids, AD organoids were smaller in size, which was shown to be caused by an increase in neuronal cell death. We also detected a higher expression of cleaved caspase-3 in the AD organoids, indicating an enhanced level of apoptosis. Thus, this disease model may be useful to investigate the potential mechanism of caspase-3 in progressive synaptic degeneration and neuronal loss in AD in future studies.

Normal calcium signaling is important to maintain brain development and function.[45−47] Destabilized calcium signaling seems to be central to the pathogenesis of Alzheimer's disease, and targeting this process might be therapeutically beneficial.[38] To investigate this process, generation of organoids that can recapitulate the functional neuronal network activity in the human brain has attracted considerable interest. Although it is challenging, several recent studies have reported inspiring results.[14,48] For example, one study showed that the cerebral organoids not only mimicked early human neurodevelopment at the cellular and molecular level, but also formed neuronal networks that could display periodic and regular oscillatory events.[48] However, experimental recapitulation of the disruption of calcium homeostasis in miniature AD organoids remains underappreciated. To fill this gap in knowledge, we analyzed neuronal network activity in AD organoids and isogenic controls, respectively. We found that synchronized Ca^{2+} transients could be observed in the neurons that migrated out from control organoids in which the $PSEN2^{N141I}$ mutation was corrected by CRISPR/Cas9 technology. This result was consistent with a previous study, which showed that cerebral organoids derived from healthy individual produced self-organized neuronal networks and exhibited spontaneous Ca^{2+} transients in synchronized patterns.[49] Additionally, we also found nonsynchronized Ca^{2+} transients in the neurons that had migrated out from the AD organoids carrying the $PSEN2^{N141I}$ mutation. This finding using the *in vitro* 3D model was well-correlated with the clinical result that there were diminished fluctuations in the level of synchronization in neural circuits from AD patients.[50,51] To the best of our knowledge, we present the first organoid-based AD model with obviously different Ca^{2+} transient patterns that are caused by a single nucleotide variation, which will be a useful system to further decipher the role of $PSEN2^{N141I}$ mutation in the regulation of calcium homeostasis in AD. Previous studies on cultured hippocampal networks demonstrated that high levels of Aβ42 significantly inhibited the synchronized spontaneous cytoplasmic Ca^{2+} transients.[52] In our study, we found that the expression level of Aβ42 was significantly increased in AD organoids, which may also contribute to the loss of synchronization of the Ca^{2+} transients. Sakaguchi and colleagues reported the formation of a self-organized and synchronized neuronal network following a dissociation culture of cerebral organoids.[49] However, in our work, once organoids were dissociated into single cells, the frequency of calcium spikes was significantly reduced, and synchronous calcium transients disappeared, indicating that the neuronal activity in 3D organoids may be more mature than that in 2D monolayer cultures.

Neuronal hyperactivity emerges early in the pathological progression of AD, in both mouse models and patients.[53] Clinical studies showed that seizures are more frequent in patients with AD compared to in healthy individuals and that

https://dx.doi.org/10.1021/acsbiomaterials.0c01583
ACS Biomater. Sci. Eng. 2021, 7, 254−264

they can hasten cognitive decline.[54] To study the potential underlying mechanism, a mouse model of AD using *in vivo* Ca^{2+} imaging revealed that AD-mediated enhancement of neuronal hyperactivity occurred mainly due to a presenilin-mediated dysfunction of intracellular Ca^{2+} stores.[55,56] Whether this functional aspect could be recapitulated *in vitro* in miniature 3D models remains unknown. Thus, we used cerebral organoids as a model to test neuronal activity by using Ca^{2+} imaging. Our results are consistent with previous studies on patients and sophisticated rodent models, showing that AD organoids carrying the $PSEN2^{N141I}$ mutation indeed displayed enhanced neuronal activity compared to the isogenic control. Therefore, alternatively, the *in vitro* organoids model also holds great potential in the study of the relationship between presenilin and neuronal hyperactivity. Moreover, this convenient and reproducible strategy can avoid the complicated surgical procedures and ethical disputes involved in *in vivo* imaging on living animals.

Neuronal cholinergic deficiency is a possible major cause of AD, which is partially linked to large reductions of choline acetyltransferase and acetylcholinesterase. So, augmentation of cholinergic neurotransmission in the brain is considered to be a potential strategy to develop drugs for the treatment of AD.[57] For example, certain compounds with the ability to enhance acetylcholine release, such as 4-AP, have shown their promising therapeutic effects on AD.[58] Wesseling and colleagues reported that 4-AP has some efficacy in improving memory and learning.[59] The derivatives of 4-AP are also under intensive investigation owing to their potential antiamnesic and cognition enhancing activities.[58] Despite these reported benefits, the use of 4-AP in the treatment of AD is still controversial. Davidson and colleagues reported that 4-AP exerted no significant effect on any particular symptoms of AD.[60] Further, the development of GABA receptor antagonists also attracted considerable attention from researchers trying to find their potential in the treatment of AD. For example, bicuculline methochloride, a GABA receptor antagonist we used in our experiments, can improve impaired synaptic plasticity and elicit neuroprotection against Aβ-mediated toxicity by blocking GABA receptors in an AD animal model.[61,62] But, so far, there is still no cure for AD, and developing therapeutics for the treatment of AD remains very complicated and challenging.[63] Therefore, many endeavors are being made to develop new drug screening platforms. Among these, 3D organoids have shown great potential in evaluating the effects of drugs due to their physiological characteristics similar to the human brain.[64] In our study, we observed that 4-AP and bicuculline methochloride could greatly increase neuronal activity in AD organoids and isogenic control organoids compared to their basal activity, indicating that organoids are responsive to these drugs. However, there was no significant difference regarding the effect of these drugs on neuronal activity between AD and i-Control organoids. Overall, our established AD organoid model has the potential to be used to screen or evaluate other types of drugs in the future.

Overall, our work has advanced our understanding of functional neuronal network activity in AD bearing a PSEN2 mutation and provided a new organoid-based *in vitro* biosystem to model human AD disease at different levels. We believe that this model will find wide applications in the near future.

■ ASSOCIATED CONTENT

Supporting Information

The Supporting Information is available free of charge at https://pubs.acs.org/doi/10.1021/acsbiomaterials.0c01583.

Immunohistochemistry staining of a pluripotent marker and neuron marker, sectioning and immunohistochemistry of Aβ42 and Aβ40, quantification of interspike distance in the i-Control and AD organoids, relative change of percentage of active neurons in the AD and i-Control organoids after TTX treatment, targeting site of sgRNA, and list of antibodies (PDF)

■ AUTHOR INFORMATION

Corresponding Author

Antonius M. VanDongen − *Program in Neuroscience and Behavioural Disorders, Duke-NUS Medical School, 169857, Singapore;* orcid.org/0000-0002-9923-3407; Email: antonius.vandongen@duke-nus.edu.sg

Author

Juan Yin − *Program in Neuroscience and Behavioural Disorders, Duke-NUS Medical School, 169857, Singapore*

Complete contact information is available at: https://pubs.acs.org/10.1021/acsbiomaterials.0c01583

Funding

This work was supported by grant NMRC/OFIRG/0019/2016 from the National Medical Research Council in Singapore.

Notes

The authors declare no competing financial interest.

■ ABBREVIATIONS

AD, Alzheimer's disease; hPSCs, human pluripotent stem cells; 3D, three-dimensional; 2D, two-dimensional; PSEN2, presenilin 2; Aβ, amyloid beta; PSEN1, presenilin 1; APP, amyloid precursor protein; i-Control, isogenic control lines; EB, embryonic body; PFA, paraformaldehyde; 4-AP, 4-aminopyridine; TTX, tetrodotoxin

■ REFERENCES

(1) Scheltens, P.; Blennow, K.; Breteler, M. M B; de Strooper, B.; Frisoni, G. B; Salloway, S.; Van der Flier, W. M.; et al. Alzheimer's disease. *Lancet* **2016**, *388* (10043), 505−517.

(2) Graham, W. V.; Bonito-Oliva, A.; Sakmar, T. P. Update on Alzheimer's disease therapy and prevention strategies. *Annu. Rev. Med.* **2017**, *68*, 413−430.

(3) Papaspyropoulos, A.; Tsolaki, M.; Foroglou, N.; Pantazaki, A. A., Modeling and Targeting Alzheimer's Disease With Organoids. *Front. Pharmacol.* **2020**, *11*. DOI: 10.3389/fphar.2020.00396

(4) Essayan-Perez, S.; Zhou, B.; Nabet, A. M.; Wernig, M.; Huang, Y.-W. A. Modeling Alzheimer's disease with human iPS cells: advancements, lessons, and applications. *Neurobiol. Dis.* **2019**, *130*, 104503.

(5) Gerakis, Y.; Hetz, C. Brain organoids: a next step for humanized Alzheimer's disease models? *Mol. Psychiatry* **2019**, *24* (4), 474−478.

(6) Kitazawa, M.; Medeiros, R.; LaFerla, F. M. Transgenic mouse models of Alzheimer disease: developing a better model as a tool for therapeutic interventions. *Curr. Pharm. Des.* **2012**, *18* (8), 1131−1147.

(7) Sasaguri, H.; Nilsson, P.; Hashimoto, S.; Nagata, K.; Saito, T.; De Strooper, B.; Hardy, J.; Vassar, R.; Winblad, B.; Saido, T. C. APP mouse models for Alzheimer's disease preclinical studies. *EMBO J.* **2017**, *36* (17), 2473−2487.

(8) Bitar, M.; Barry, G. Building a Human Brain for Research. *Front. Mol. Neurosci.* **2020**, *13*, 22.
(9) Yagi, T.; Ito, D.; Okada, Y.; Akamatsu, W.; Nihei, Y.; Yoshizaki, T.; Yamanaka, S.; Okano, H.; Suzuki, N. Modeling familial Alzheimer's disease with induced pluripotent stem cells. *Hum. Mol. Genet.* **2011**, *20* (23), 4530−9.
(10) Israel, M. A.; Yuan, S. H.; Bardy, C.; Reyna, S. M.; Mu, Y.; Herrera, C.; Hefferan, M. P.; Van Gorp, S.; Nazor, K. L.; Boscolo, F. S.; Carson, C. T.; Laurent, L. C.; Marsala, M.; Gage, F. H.; Remes, A. M.; Koo, E. H.; Goldstein, L. S. Probing sporadic and familial Alzheimer's disease using induced pluripotent stem cells. *Nature* **2012**, *482* (7384), 216−20.
(11) Arber, C.; Lovejoy, C.; Wray, S. Stem cell models of Alzheimer's disease: progress and challenges. *Alzheimer's Res. Ther.* **2017**, *9* (1), 42.
(12) Israel, M. A.; Yuan, S. H.; Bardy, C.; Reyna, S. M.; Mu, Y.; Herrera, C.; Hefferan, M. P.; Van Gorp, S.; Nazor, K. L.; Boscolo, F. S. Probing sporadic and familial Alzheimer's disease using induced pluripotent stem cells. *Nature* **2012**, *482* (7384), 216−220.
(13) Weber, R. J.; Cerchiari, A. E.; Delannoy, L. S.; Garbe, J. C.; LaBarge, M. A.; Desai, T. A.; Gartner, Z. J. Rapid Organoid Reconstitution by Chemical Micromolding. *ACS Biomater. Sci. Eng.* **2016**, *2* (11), 1851−1855.
(14) Cantley, W. L.; Du, C.; Lomoio, S.; DePalma, T.; Peirent, E.; Kleinknecht, D.; Hunter, M.; Tang-Schomer, M. D.; Tesco, G.; Kaplan, D. L. Functional and Sustainable 3D Human Neural Network Models from Pluripotent Stem Cells. *ACS Biomater. Sci. Eng.* **2018**, *4* (12), 4278−4288.
(15) Choi, S. H.; Kim, Y. H.; Hebisch, M.; Sliwinski, C.; Lee, S.; D'Avanzo, C.; Chen, H.; Hooli, B.; Asselin, C.; Muffat, J.; Klee, J. B.; Zhang, C.; Wainger, B. J.; Peitz, M.; Kovacs, D. M.; Woolf, C. J.; Wagner, S. L.; Tanzi, R. E.; Kim, D. Y. A three-dimensional human neural cell culture model of Alzheimer's disease. *Nature* **2014**, *515* (7526), 274−8.
(16) Raja, W. K.; Mungenast, A. E.; Lin, Y. T.; Ko, T.; Abdurrob, F.; Seo, J.; Tsai, L. H. Self-Organizing 3D Human Neural Tissue Derived from Induced Pluripotent Stem Cells Recapitulate Alzheimer's Disease Phenotypes. *PLoS One* **2016**, *11* (9), No. e0161969.
(17) Gonzalez, C.; Armijo, E.; Bravo-Alegria, J.; Becerra-Calixto, A.; Mays, C. E.; Soto, C. Modeling amyloid beta and tau pathology in human cerebral organoids. *Mol. Psychiatry* **2018**, *23* (12), 2363−2374.
(18) Yin, F.; Zhu, Y.; Wang, Y.; Qin, J. Engineering Brain Organoids to Probe Impaired Neurogenesis Induced by Cadmium. *ACS Biomater. Sci. Eng.* **2018**, *4* (5), 1908−1915.
(19) Mansour, A. A.; Gonçalves, J. T.; Bloyd, C. W.; Li, H.; Fernandes, S.; Quang, D.; Johnston, S.; Parylak, S. L.; Jin, X.; Gage, F. H. An in vivo model of functional and vascularized human brain organoids. *Nat. Biotechnol.* **2018**, *36* (5), 432.
(20) Cai, Y.; An, S. S.; Kim, S. Mutations in presenilin 2 and its implications in Alzheimer's disease and other dementia-associated disorders. *Clin. Interventions Aging* **2015**, *10*, 1163−72.
(21) Moreno, C. L.; Della Guardia, L.; Shnyder, V.; Ortiz-Virumbrales, M.; Kruglikov, I.; Zhang, B.; Schadt, E. E.; Tanzi, R. E.; Noggle, S.; Buettner, C.; Gandy, S. iPSC-derived familial Alzheimer's PSEN2 (N141I) cholinergic neurons exhibit mutation-dependent molecular pathology corrected by insulin signaling. *Mol. Neurodegener.* **2018**, *13* (1), 33.
(22) Sannerud, R.; Esselens, C.; Ejsmont, P.; Mattera, R.; Rochin, L.; Tharkeshwar, A. K.; De Baets, G.; De Wever, V.; Habets, R.; Baert, V. Restricted location of PSEN2/γ-secretase determines substrate specificity and generates an intracellular Aβ pool. *Cell* **2016**, *166* (1), 193−208.
(23) Chen, Y.; Cao, J.; Xiong, M.; Petersen, A. J.; Dong, Y.; Tao, Y.; Huang, C. T.; Du, Z.; Zhang, S. C. Engineering Human Stem Cell Lines with Inducible Gene Knockout using CRISPR/Cas9. *Cell Stem Cell* **2015**, *17* (2), 233−44.
(24) Cai, Y.; An, S. S. A.; Kim, S. Mutations in presenilin 2 and its implications in Alzheimer's disease and other dementia-associated disorders. *Clin. Interventions Aging* **2015**, *10*, 1163.
(25) Lancaster, M. A.; Renner, M.; Martin, C.-A.; Wenzel, D.; Bicknell, L. S.; Hurles, M. E.; Homfray, T.; Penninger, J. M.; Jackson, A. P.; Knoblich, J. A. Cerebral organoids model human brain development and microcephaly. *Nature* **2013**, *501* (7467), 373.
(26) Lancaster, M. A.; Knoblich, J. A. Generation of cerebral organoids from human pluripotent stem cells. *Nat. Protoc.* **2014**, *9* (10), 2329.
(27) Lancaster, M. A.; Knoblich, J. A. Organogenesis in a dish: modeling development and disease using organoid technologies. *Science* **2014**, *345* (6194), 1247125.
(28) Paşca, A. M.; Sloan, S. A.; Clarke, L. E.; Tian, Y.; Makinson, C. D.; Huber, N.; Kim, C. H.; Park, J.-Y.; O'rourke, N. A.; Nguyen, K. D. Functional cortical neurons and astrocytes from human pluripotent stem cells in 3D culture. *Nat. Methods* **2015**, *12* (7), 671.
(29) Kadoshima, T.; Sakaguchi, H.; Nakano, T.; Soen, M.; Ando, S.; Eiraku, M.; Sasai, Y. Self-organization of axial polarity, inside-out layer pattern, and species-specific progenitor dynamics in human ES cell−derived neocortex. *Proc. Natl. Acad. Sci. U. S. A.* **2013**, *110* (50), 20284−20289.
(30) Kumar-Singh, S.; Theuns, J.; Van Broeck, B.; Pirici, D.; Vennekens, K.; Corsmit, E.; Cruts, M.; Dermaut, B.; Wang, R.; Van Broeckhoven, C. Mean age-of-onset of familial alzheimer disease caused by presenilin mutations correlates with both increased Abeta42 and decreased Abeta40. *Hum. Mutat.* **2006**, *27* (7), 686−95.
(31) Scopa, C.; Marrocco, F.; Latina, V.; Ruggeri, F.; Corvaglia, V.; La Regina, F.; Ammassari-Teule, M.; Middei, S.; Amadoro, G.; Meli, G.; Scardigli, R.; Cattaneo, A. Impaired adult neurogenesis is an early event in Alzheimer's disease neurodegeneration, mediated by intracellular Aβ oligomers. *Cell Death Differ.* **2020**, *27* (3), 934−948.
(32) Pini, L.; Pievani, M.; Bocchetta, M.; Altomare, D.; Bosco, P.; Cavedo, E.; Galluzzi, S.; Marizzoni, M.; Frisoni, G. B. Brain atrophy in Alzheimer's disease and aging. *Ageing Res. Rev.* **2016**, *30*, 25−48.
(33) Caccamo, A.; Branca, C.; Piras, I. S.; Ferreira, E.; Huentelman, M. J.; Liang, W. S.; Readhead, B.; Dudley, J. T.; Spangenberg, E. E.; Green, K. N. Necroptosis activation in Alzheimer's disease. *Nat. Neurosci.* **2017**, *20* (9), 1236.
(34) Su, J. H.; Zhao, M.; Anderson, A. J.; Srinivasan, A.; Cotman, C. W. Activated caspase-3 expression in Alzheimer's and aged control brain: correlation with Alzheimer pathology. *Brain Res.* **2001**, *898* (2), 350−357.
(35) Alves da Costa, C.; Paitel, E.; Mattson, M. P.; Amson, R.; Telerman, A.; Ancolio, K.; Checler, F. Wild-type and mutated presenilins 2 trigger p53-dependent apoptosis and down-regulate presenilin 1 expression in HEK293 human cells and in murine neurons. *Proc. Natl. Acad. Sci. U. S. A.* **2002**, *99* (6), 4043−4048.
(36) Giandomenico, S. L.; Mierau, S. B.; Gibbons, G. M.; Wenger, L. M. D.; Masullo, L.; Sit, T.; Sutcliffe, M.; Boulanger, J.; Tripodi, M.; Derivery, E.; Paulsen, O.; Lakatos, A.; Lancaster, M. A. Cerebral organoids at the air-liquid interface generate diverse nerve tracts with functional output. *Nat. Neurosci.* **2019**, *22* (4), 669−679.
(37) Quadrato, G.; Nguyen, T.; Macosko, E. Z.; Sherwood, J. L.; Min Yang, S.; Berger, D. R.; Maria, N.; Scholvin, J.; Goldman, M.; Kinney, J. P.; Boyden, E. S.; Lichtman, J. W.; Williams, Z. M.; McCarroll, S. A.; Arlotta, P. Cell diversity and network dynamics in photosensitive human brain organoids. *Nature* **2017**, *545* (7652), 48−53.
(38) LaFerla, F. M. Calcium dyshomeostasis and intracellular signalling in Alzheimer's disease. *Nat. Rev. Neurosci.* **2002**, *3* (11), 862−872.
(39) Leung, H.-W.; Foo, G. W. Q.; VanDongen, A. M. Arc Regulates Transcription of Genes for Plasticity, Excitability and Alzheimer's Disease. *bioRxiv* **2019**, 833988.
(40) Opitz, T.; De Lima, A. D.; Voigt, T. Spontaneous development of synchronous oscillatory activity during maturation of cortical networks in vitro. *J. Neurophysiol.* **2002**, *88* (5), 2196−2206.
(41) Lancaster, M. A.; Renner, M.; Martin, C. A.; Wenzel, D.; Bicknell, L. S.; Hurles, M. E.; Homfray, T.; Penninger, J. M.; Jackson, A. P.; Knoblich, J. A. Cerebral organoids model human brain development and microcephaly. *Nature* **2013**, *501* (7467), 373−9.

https://dx.doi.org/10.1021/acsbiomaterials.0c01583
ACS Biomater. Sci. Eng. 2021, 7, 254−264

(42) Amin, N. D.; Pasca, S. P. Building Models of Brain Disorders with Three-Dimensional Organoids. *Neuron* **2018**, *100* (2), 389−405.
(43) Iefremova, V.; Manikakis, G.; Krefft, O.; Jabali, A.; Weynans, K.; Wilkens, R.; Marsoner, F.; Brandl, B.; Muller, F. J.; Koch, P.; Ladewig, J. An Organoid-Based Model of Cortical Development Identifies Non-Cell-Autonomous Defects in Wnt Signaling Contributing to Miller-Dieker Syndrome. *Cell Rep.* **2017**, *19* (1), 50−59.
(44) Thomas, C. A.; Tejwani, L.; Trujillo, C. A.; Negraes, P. D.; Herai, R. H.; Mesci, P.; Macia, A.; Crow, Y. J.; Muotri, A. R. Modeling of TREX1-Dependent Autoimmune Disease using Human Stem Cells Highlights L1 Accumulation as a Source of Neuroinflammation. *Cell Stem Cell* **2017**, *21* (3), 319−331.
(45) Rosenberg, S. S.; Spitzer, N. C. Calcium signaling in neuronal development. *Cold Spring Harb Perspect Biol.* **2011**, *3* (10), No. a004259.
(46) Kawamoto, E. M.; Vivar, C.; Camandola, S. Physiology and pathology of calcium signaling in the brain. *Front. Pharmacol.* **2012**, *3*, 61−61.
(47) Marambaud, P.; Dreses-Werringloer, U.; Vingtdeux, V. Calcium signaling in neurodegeneration. *Mol. Neurodegener.* **2009**, *4*, 20.
(48) Trujillo, C. A.; Gao, R.; Negraes, P. D.; Gu, J.; Buchanan, J.; Preissl, S.; Wang, A.; Wu, W.; Haddad, G. G.; Chaim, I. A.; Domissy, A.; Vandenberghe, M.; Devor, A.; Yeo, G. W.; Voytek, B.; Muotri, A. R. Complex Oscillatory Waves Emerging from Cortical Organoids Model Early Human Brain Network Development. *Cell Stem Cell* **2019**, *25* (4), 558−569.
(49) Sakaguchi, H.; Ozaki, Y.; Ashida, T.; Matsubara, T.; Oishi, N.; Kihara, S.; Takahashi, J. Self-Organized Synchronous Calcium Transients in a Cultured Human Neural Network Derived from Cerebral Organoids. *Stem Cell Rep.* **2019**, *13* (3), 458−473.
(50) Koenig, T.; Prichep, L.; Dierks, T.; Hubl, D.; Wahlund, L. O.; John, E. R.; Jelic, V. Decreased EEG synchronization in Alzheimer's disease and mild cognitive impairment. *Neurobiol. Aging* **2005**, *26* (2), 165−171.
(51) Stam, C. J.; Montez, T.; Jones, B. F.; Rombouts, S. A. R. B.; van der Made, Y.; Pijnenburg, Y. A. L.; Scheltens, P. Disturbed fluctuations of resting state EEG synchronization in Alzheimer's disease. *Clin. Neurophysiol.* **2005**, *116* (3), 708−715.
(52) Rui, Y.; Li, R.; Liu, Y.; Zhu, S.; Yu, X.; Sheng, Z.; Xie, Z. Acute effect of beta amyloid on synchronized spontaneous Ca2+ oscillations in cultured hippocampal networks. *Cell Biol. Int.* **2006**, *30* (9), 733−40.
(53) Busche, M. A.; Grienberger, C.; Keskin, A. D.; Song, B.; Neumann, U.; Staufenbiel, M.; Forstl, H.; Konnerth, A. Decreased amyloid-beta and increased neuronal hyperactivity by immunotherapy in Alzheimer's models. *Nat. Neurosci.* **2015**, *18* (12), 1725−7.
(54) Vossel, K. A.; Ranasinghe, K. G.; Beagle, A. J.; Mizuiri, D.; Honma, S. M.; Dowling, A. F.; Darwish, S. M.; Van Berlo, V.; Barnes, D. E.; Mantle, M.; Karydas, A. M.; Coppola, G.; Roberson, E. D.; Miller, B. L.; Garcia, P. A.; Kirsch, H. E.; Mucke, L.; Nagarajan, S. S. Incidence and impact of subclinical epileptiform activity in Alzheimer's disease. *Ann. Neurol.* **2016**, *80* (6), 858−870.
(55) Lerdkrai, C.; Asavapanumas, N.; Brawek, B.; Kovalchuk, Y.; Mojtahedi, N.; Olmedillas Del Moral, M.; Garaschuk, O. Intracellular Ca(2+) stores control in vivo neuronal hyperactivity in a mouse model of Alzheimer's disease. *Proc. Natl. Acad. Sci. U. S. A.* **2018**, *115* (6), E1279−E1288.
(56) Ghatak, S.; Dolatabadi, N.; Trudler, D.; Zhang, X.; Wu, Y.; Mohata, M.; Ambasudhan, R.; Talantova, M.; Lipton, S. A., Mechanisms of hyperexcitability in Alzheimer's disease hiPSC-derived neurons and cerebral organoids vs isogenic controls. *eLife* **2019**, *8*. DOI: 10.7554/eLife.50333
(57) Shrivastava, S. K.; Sinha, S. K.; Srivastava, P.; Tripathi, P. N.; Sharma, P.; Tripathi, M. K.; Tripathi, A.; Choubey, P. K.; Waiker, D. K.; Aggarwal, L. M. Design and development of novel p-aminobenzoic acid derivatives as potential cholinesterase inhibitors for the treatment of Alzheimer's disease. *Bioorg. Chem.* **2019**, *82*, 211−223.
(58) Andreani, A.; Leoni, A.; Locatelli, A.; Morigi, R.; Rambaldi, M.; Pietra, C.; Villetti, G. 4-Aminopyridine derivatives with antiamnesic activity. *Eur. J. Med. Chem.* **2000**, *35* (1), 77−82.
(59) Wesseling, H.; Agoston, S.; Van Dam, G.; Pasma, J.; DeWit, D.; Havinga, H. Effects of 4-aminopyridine in elderly patients with Alzheimer's disease. *N. Engl. J. Med.* **1984**, *310* (15), 988.
(60) Davidson, M.; Zemishlany, Z.; Mohs, R. C.; Horvath, T. B.; Powchik, P.; Blass, J. P.; Davis, K. L. 4-Aminopyridine in the treatment of Alzheimer's disease. *Biol. Psychiatry* **1988**, *23* (5), 485−490.
(61) Lee, B. Y.; Ban, J. Y.; Seong, Y. H. Chronic stimulation of GABAA receptor with muscimol reduces amyloid β protein (25−35)-induced neurotoxicity in cultured rat cortical cells. *Neurosci. Res.* **2005**, *52* (4), 347−356.
(62) Kadoyama, K.; Matsuura, K.; Takano, M.; Otani, M.; Tomiyama, T.; Mori, H.; Matsuyama, S., Proteomic analysis involved with synaptic plasticity improvement by GABAA receptor blockade in hippocampus of a mouse model of Alzheimer's disease. *Neurosci. Res.* **2020**. DOI: 10.1016/j.neures.2020.04.004
(63) Frozza, R. L.; Lourenco, M. V.; De Felice, F. G., Challenges for Alzheimer's Disease Therapy: Insights from Novel Mechanisms Beyond Memory Defects. *Frontiers in Neuroscience* **2018**, *12* (37).
(64) Takahashi, T. Organoids for Drug Discovery and Personalized Medicine. *Annu. Rev. Pharmacol. Toxicol.* **2019**, *59* (1), 447−462.

https://dx.doi.org/10.1021/acsbiomaterials.0c01583
ACS Biomater. Sci. Eng. 2021, 7, 254−264